Journal of Materials Chemistry A

Accepted Manuscript

ROYAL SOCIETY OF CHEMISTRY

www.rsc.org/materialsA

Enhanced Reactivity of High-index Surface Platinum Hollow Nanocrystals

Edgar González[1,2,3], Florind Merkoçi[1], Raúl Arenal[4,5], Jordi Arbiol[6,7], Joan Esteve[8], Neus G. Bastús[1] and Víctor Puntes[1,7*]

[1]Institut Català de Nanotecnologia (ICN), Campus de la UAB, 08193 Bellaterra, Spain.
[2]Centro de Ciencia y Tecnología Nanoescalar, 111311 Bogotá, Colombia.
[3]Facultad de Ingeniería, Instituto Geofísico Pontificia Universidad Javeriana, 110231 Bogotá, Colombia.
[4]Instituto de Nanociencia de Aragon, Universidad de Zaragoza, 50018 Zaragoza, Spain.
[5]ARAID Foundation, Paseo Maria Agustin, 36, 50004 Zaragoza, Spain.
[6]Institut de Ciència de Materials de Barcelona (ICMAB-CSIC), Campus de la UAB, 08193 Bellaterra, Spain.
[7]Institució Catalana de Recerca i Estudis Avançats (ICREA), 08010 Barcelona, Spain.
[8]Departament de Física Aplicada i Óptica, Universitat de Barcelona, 08028, Barcelona, Spain.

[*]To whom correspondence should be addressed: E-mail: victor.puntes@icn.cat

Keywords: Hollow Nanocrystals, Surface Engineering, Galvanic Replacement, Surface Reactive, Room Temperature.

Abstract

The precise morphological control of the surface of inorganic nanocrystals (NCs) is critical for the understanding of the unique properties of the materials at the nanoscale and useful in a wide range of applications, such as catalysis, where the development highly active and low-cost materials represents a landmark for the development of industrial technologies. Here we show how combining solid state chemistry and colloidal synthesis allows us to prepare exotic materials, in particular, PtAg@Pt single-crystal hollow NCs with high-index planes synthesized at room temperature by controlled corrosion of silver templates, which minimize Pt consumption and maximize surface reactivity.

Introduction

Noble metal nanocrystals (NCs) have been extensively studied recently because of their promising wide application range owing to their intriguing optical and electronic properties, which arise from their constitutional and precise morphological variations. This is dramatic in the case of heterogeneous catalysis, where low-coordination surface atomic sites are largely responsible for the observed behavior.[1, 2] Consequently, it is known that the catalytic properties of metal and alloy NCs strongly depend on atomic local features as coordination and crystallographic index planes, which in turn are determined by the method of preparation.[3-5] A very important case is that of the *expensive rare* metal Pt and its widespread use in low temperature polymer electrolyte (proton exchange) membrane fuel cells[6]. Consequently, very small NCs (< 5 nm) to maximize surface to volume (mass) ratio have been synthesized to increase the (economic) competitiveness of these material. However, such small NCs are unstable and tend to sinter or detach from the support during operation.[7, 8] This has fuelled up investigation on hollow Pt NCs, as an efficient alternative to increase the surface to mass ratio.[7, 9-11] Initially, Pt hollow NCs were prepared by galvanic replacement using Co[12] and Ag templates.[13] Due to the high immiscibility of Ag and Pt at low T, NCs with very rough surfaces where obtained when Pt had to grow on top of Ag. Because of that, other groups prepared Pd templates to produce Pt hollow NCs with smoother surfaces.[14, 15] Recently, ultrathin (down to 3 atomic layers) Pt hollow NCs have been prepared reaching a new limit in the optimization of the surface to mass ratio of Pt NCs.[16] In addition of reducing effective mass, the increase of surface activity per unit area is also a good strategy to increase Pt NCs performance. Indeed, it is well known that for most catalytic reactions, high-index planes (low coordinated atoms), associated with atomic steps, edges and kinks have been considered the responsible for the enhancement of catalytic performance.[2] Thus, high-index surface Pt-based

NCs have been sought and prepared showing strong thermal and chemical stability and enhanced catalytic activity (up to 400%).[2, 17, 18]

In order to produce stable high-index faceted NCs, we observed that the processes of dissolution and deposition during galvanic replacement reactions could be used to control the atomic roughness of the NCs and promote the alloying of Pt and Ag despite their immiscibility.[11] It is important to note that solid state diffusion processes are dramatically enhanced at the nanoscale (up to 10 orders of magnitude[19]). Thus, corrosion processes at the nanoscale show concomitant diffusion and migration of atoms in the solid matrix, allowing the production of designed materials by unexpected ways. This is the case of transformations of NC's composition while maintaining their morphological integrity[20] or the carving of complex patterns in multimetallic hollow NCs,[19] where the void is an added degree of freedom to control morphology in a regime where structure as much as composition determines activity. This plasticity manifested in enhanced diffusion coefficients, [19, 21, 22] has been also observed in the high tolerance to crystal strain,[23] low tolerance to crystal defects,[24] decrease of the melting temperature, and the easiness for defect curing in NCs.[25, 26] Here we show how to prepare different hollow Pt NCs and specially PtAg@Pt single-crystals showing stable high-index planes (such as {950}, {910}, {540} and/or {4-10}) synthesized at room temperature by controlled corrosion of silver templates, which minimize Pt consumption and maximize surface reactivity. We would like to note that

Results and Discussion

Platinum NCs grown onto silver templates tend to grow in a Volmer-Weber (island by island) mode due to their lattice mismatch and high immiscibility at low T. Therefore, normally, few nm (2-3 nm) rough Pt NC surfaces are obtained when Ag templates are used,[9, 13] as those shown in **Figure 1a**. Thus, to promote PtAg alloying and a more epitaxial growth, several strategies were employed allowing metal inter-diffusion to play a significant role during NC

synthesis.[27, 28] First, the work at low temperature, the use of insoluble platinum salts, where Pt^{2+} is slowly solubilized and consumed, maintaining a low (but constant) concentration of reactive Pt in solution, and the use of mild reducing agents with the intention of reducing Pt^{2+} avidity for Ag 5s electrons. It is also worth noting that in the mixture, as a by-product, there is the generation of highly insoluble AgCl and AgBr compounds, which here are solubilized by the presence of surfactants.[19] As a consequence of this reaction conditions, the island growth mode (rough surfaces) is avoided and interdiffusion is promoted allowing the formation of NC smooth surfaces exposing high index planes and PtAg alloys (**Fig. 1d**).

Thus, by using silver NCs as sacrificial templates, polyvinylpyrrolidone (PVP), benzylalkyldimethylammonium chloride (BDAC) and cetyltrymethylamonium bromide (CTAB) as surfactants and complexing agents, platinum salts (K_2PtCl4, H_2PtCl_6, $PtCl_2$) as precursors and oxidizing agents, and ascorbic acid as reducing agent, distinct hollow PtAg and Pt NCs were obtained (**Fig 1**). We observed that Pt dosing was critical to control the reaction towards the desired products. Initially, when using K_2PtCl_4 as a precursor, controlled corrosion was not achieved (**Fig. S1c**). However, when a more oxidizing form of Pt (H_2PtCl_6) was used, PtAg hollow nanoflowers with symmetrically distributed pores were systematically obtained (**Fig. 1b**). By modifying the reaction conditions, using CTAB as surfactant and $PtCl_2$ as precursor, which is poorly soluble in water, hollow NCs were formed displaying the formation of Pt islands at the NC rough surface (**Fig. 1a**), as witness of a Volmer-Weber type of growth due to the low affinity of the substrate for the deposited material.[29] This mode of growth can be seen when using a number of surfactants and precursors (**Fig. S2**). In those cases, as expected, no degree of PtAg alloying was observed. However, using BDAC as surfactant and $PtCl_2$ as precursor resulted in the formation of single-crystal nanoboxes with smooth surfaces exhibiting high-index atomic planes, forming a stable and homogeneous alloy between Ag and Pt, coated by a thin overlayer of pure platinum (PtAg@Pt hollow NCs)

(**Fig. 1d** and **Fig. 2**). Here, it seems that the Volmer-Weber growth was suppressed allowing an atom-by-atom Pt growth to take place.

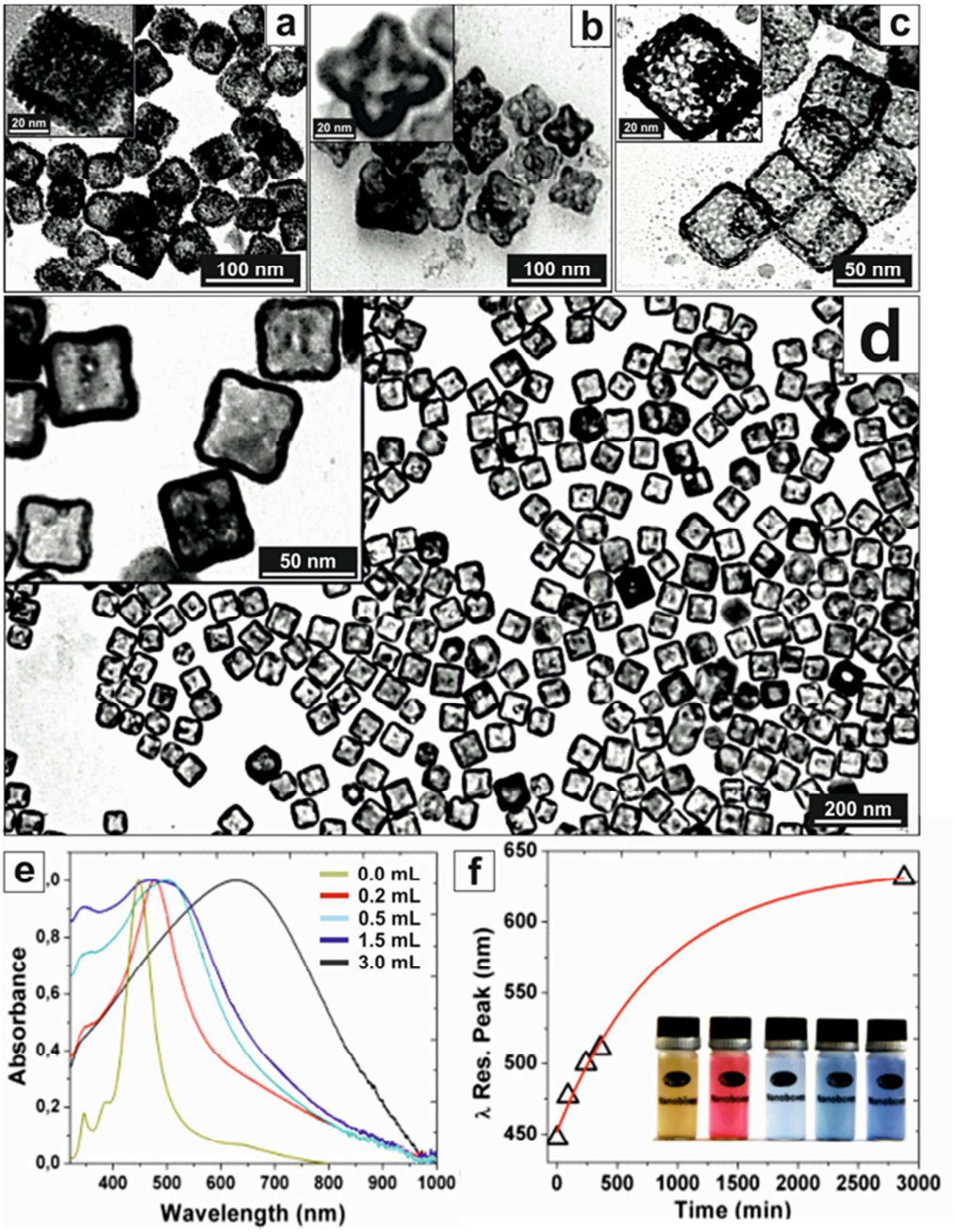

Figure 1. TEM images of hollow **a)** PtAg nanoflowers prepared by using H_2PtCl_6 as precursor and BDAC as surfactant, **b)** Volmer-Weber type (island growth) of rough surface nanoboxes synthesized by using $PtCl_2$ as precursor and CTAB as surfactant. **c)** PtAg dealloyed nanocages prepared by adding an excess of Pt salt. **d)** PtAg@Pt alloy smooth surface nanoboxes prepared by using $PtCl_2$ as precursor and BDAC as surfactant, and **e)** UV-

vis spectra for different volumes of added precursor (1mM). **f**) Time evolution of UV-VIS resonance position peak during of the formation of the nanoboxes shown in d).

In our conditions, the formation of these hollow NCs took up to 50 hours. Aliquots taken at intermediate times of the reaction showed intermediate corrosion states, in which we could appreciate also the formation of Kirkendall voids that disappeared in the final product (**Fig. S1**). Finally, further oxidation of these structures with Pt^{2+} led to PtAg dealloying and the formation of highly porous Pt nanocages (**Fig. 1c**). During this time the colour of the solution changed with a strong redshift and a dramatic broadening of the absorbance spectrum, indicative of the formation of plasmonic cavities[13, 30-32] (**Fig. 1e,f**). Note that these observed absorption bands are different from those obtained in other reported Pt-Ag NCs, which indeed consisted of layers of metals rather than a mixture (alloy) at the atomic level.[33]

Figure 2 shows high-resolution TEM images of the obtained PtAg@Pt smooth surface hollow NCs. The outer surface roughness is composed of monoatomic steps leading to highly reactive high-index surfaces (**Fig. 2d-f,** and **Figs. S3, S4**) associated to a known higher catalytic activity.[2, 17, 34] The atomic representation extracted from the atomic-resolved image corresponds to the 2D projection of the 3D structure. Therefore, the real roughness is smoothed by this integration and the real atom de-coordination (or very low coordination) is even higher. Note that for standard high performant Pt NCs their surface is much smoother.[16, 35] For comparison, an example of a perfect {100} solid Pt nanocube of similar dimensions showing monoatomic flat surfaces[36, 37] is presented (**Fig. S5**). All these studied nanoboxes are monocrystalline (**Fig. 2c**) and narrowly dispersed with no other by-product present in the synthesis solution (**Fig. 1d**).

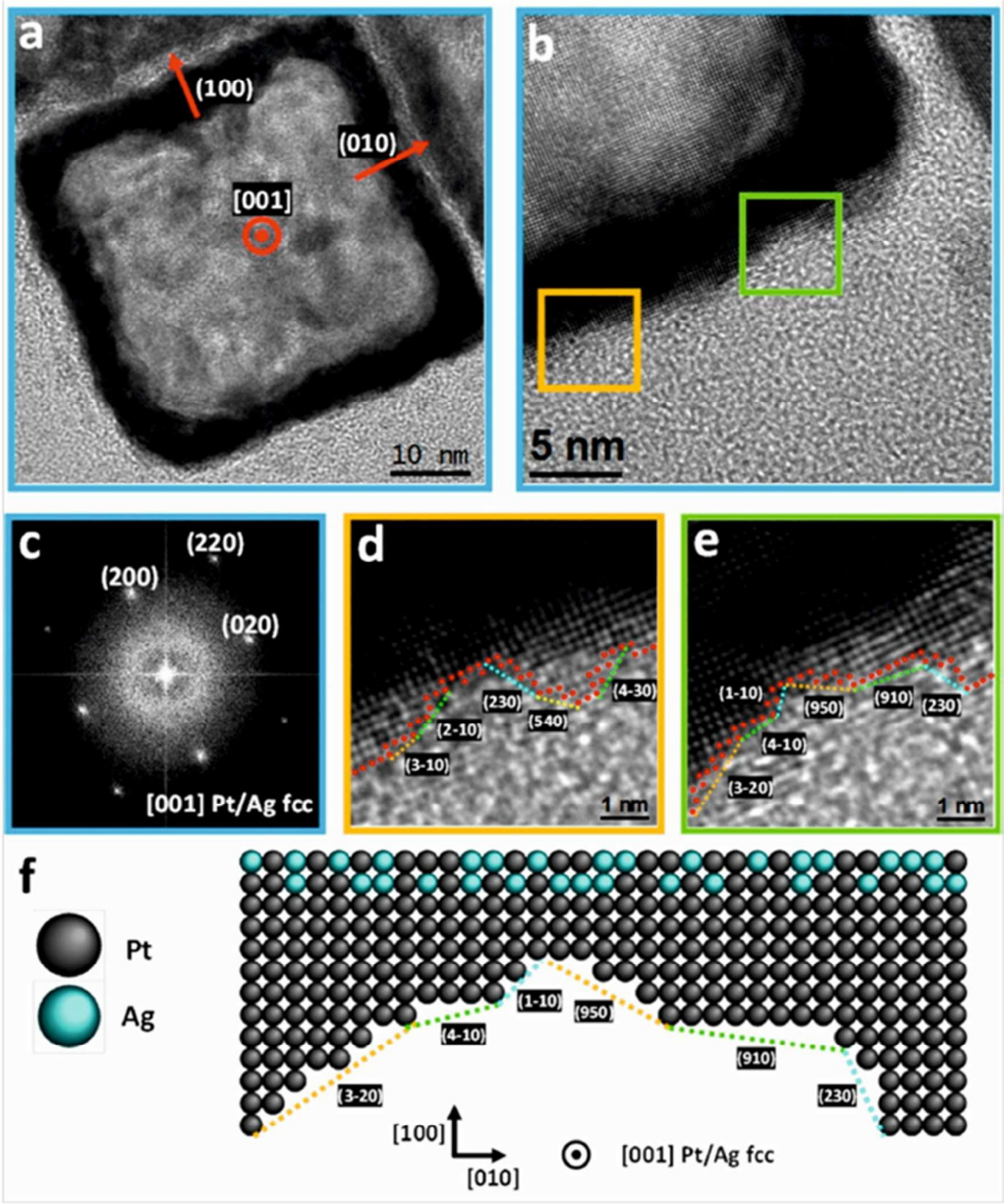

Figure 2. a), b) HRTEM image for hollow PtAg@Pt nanoboxes synthesized at room temperature. The roughness is composed of monoatomic steps leading to high-index surfaces. **c)** The power spectrum (FFT) shows that the NCs are monocrystalline and that no extra crystals are present. **d), e)** Enlarged view of the yellow (lower left) and green (higher right) areas in b). The red dots indicate the Pt atoms. **f)** Schematic representation of e) with alternating (yellow, green, cyan) colours indicating the resulting projected stepped high-index crystal planes, along with their plane indices.

In **Figure 3** we present a detailed high-resolution Energy-Dispersive X-Ray Spectroscopy (EDS) analysis on one of the lateral facets of a representative PtAg@Pt nanobox. The wall has a thickness of around 5 nm, the first -inner- 2.5 nm are composed of a PtAg alloy while the external –outer- 2.5nm surface is mainly composed of Pt, as observed in the maps and the EDS profile (**Fig. 3a-c**). This anisotropy, together with the formation of a stable PtAg solid solution are indicative footprints of the synthetic process. It is known that Pt in the bulk form does not readily undergo solid-solid diffusion with Ag at temperatures below 900 K.[13]

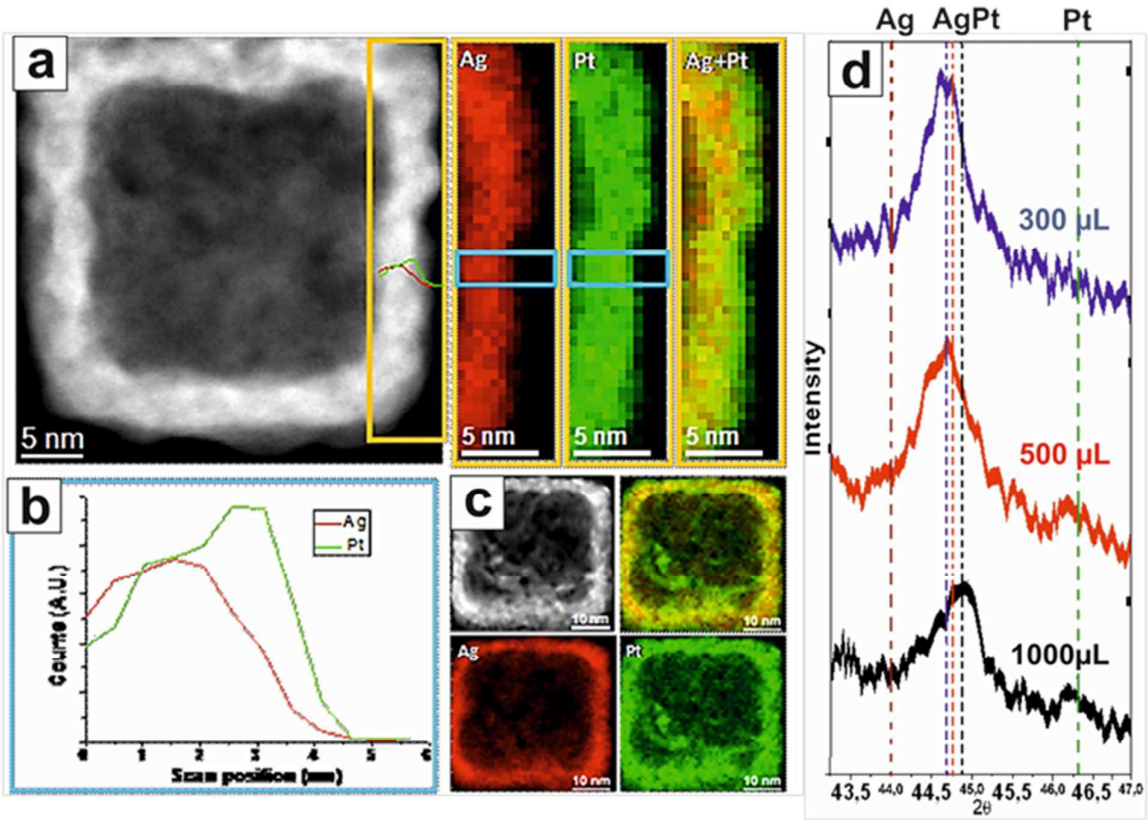

Figure 3. a) HAADF (S)TEM view of a PtAg@Pt nanobox. Right insets show detailed EDS analysis on one of the lateral walls. **b)** EDS profile. **c)** Full nanobox EDS maps. **d)** XRD (111) peak of PtAg@Pt nanoboxes for different volumes of Pt precursor added (1 mM) . The diffraction peaks fall between the values for pure platinum (green dashes) and silver (red dashes) indicating it is a metal alloy. Dashed (blue, red and black) lines indicate the diffraction peak's position for each added volume of Pt precursor, where can be seen its displacement towards the pure platinum value as the Pt/Ag ratio increases.

However, theoretical studies, and some limited experimental data have shown that miscibility between metal elements can be significantly altered at the nanoscale, including formation of PtAg alloys in the immiscible area,[38-40] despite their different reduction kinetics and thermodynamic immiscibility. In fact, due to the higher number of vacancies and enhanced mobility at the nanoscale,[24] the formation of large PtAg-alloy single crystals at RT is enabled. Of course, when forced to mix at RT, Pt and Ag should relax the consequent crystal strains into highly atomic-uneven surfaces. These PtAg alloy NCs are then passivated and stabilized with a final Pt deposition (~2-3 nm) which seals all the open Galvanic gaps, as it is in the case of the original reported Au nanoboxes.[41] The PtAg alloy at RT is forcedly strained and therefore serves as a substrate for the deposition of the high-index Pt facets. The formation of the PtAg alloy is confirmed by the EDS spectra and the XRD patterns (**Fig. 3d** and **Fig. S6**).

This synthetic strategy can be applied to different Pt/Ag compositions (**Fig. 3d** and **Figs. S6, S7**) and sacrificial templates (**Fig. 4**). Thus, using Ag spheres or wires as templates, both the immiscible Volmer-Weber (rough) growth and the generation of (smooth) PtAg@Pt single crystal hollow spheres and tubes could be obtained (**Fig. 4**). It is important to note that Pt nanotubes, because of their shape and aspect ratio are very appealing since they could act, for example, as both catalyst and electrode in fuel cells, where one main drawback is the degradation of the C electrodes that support the Pt catalytic centers.[42]

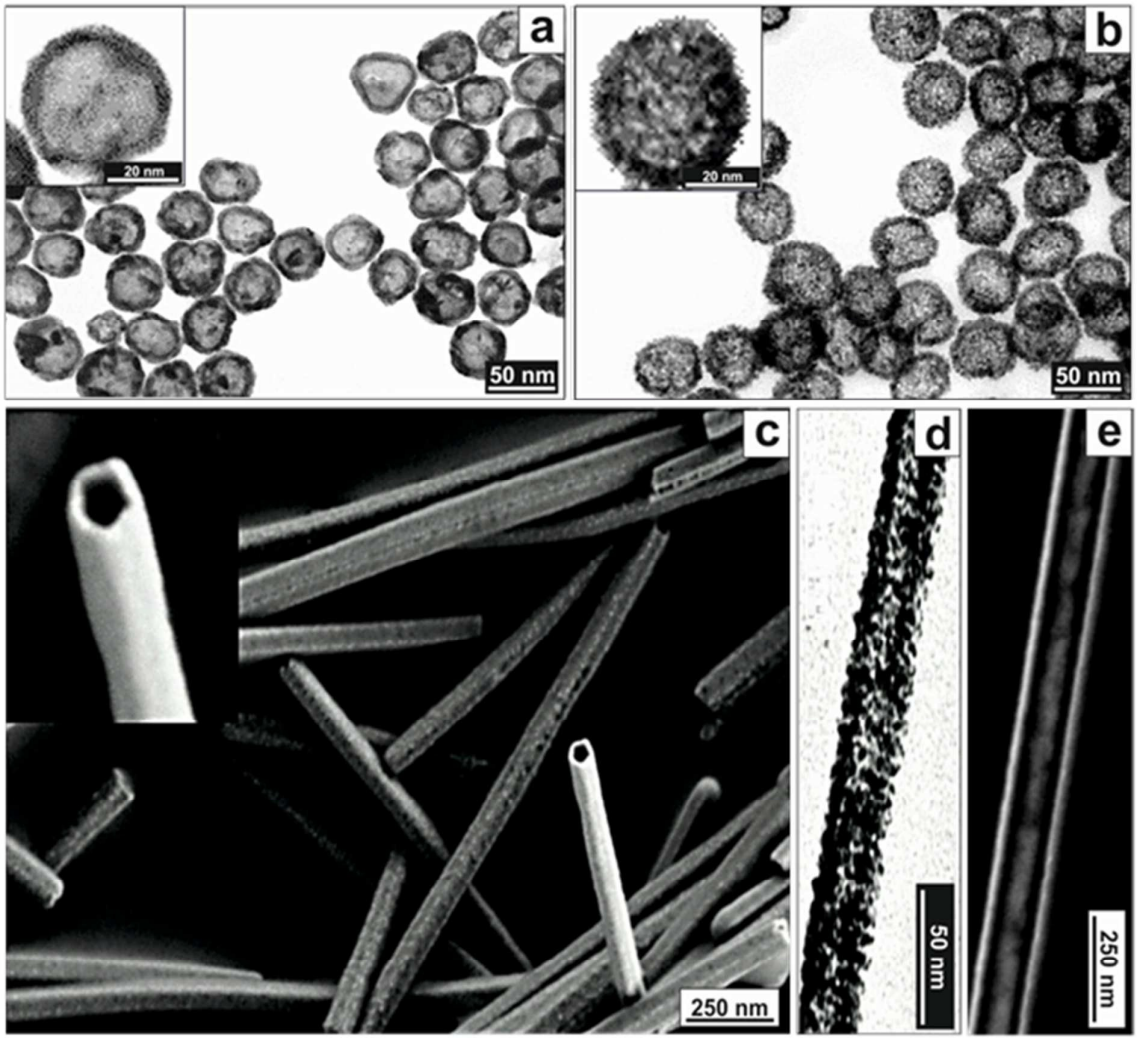

Figure 4. TEM images of spherical **a)** smooth surface PtAg NCs and **b**) rough surface Volmer-Weber type of grown NCs, both prepared by using K_2PtCl_4 as precursor and PVP as surfactant at different molar ratios. **c)** and **e)** show SEM and (S)TEM images, respectively, of smooth surface PtAg nanotubes that can be obtained with $PtCl_2$ as precursor and CTAB as surfactant or with K_2PtCl_4 as precursor and PVP as surfactant, while **d)** shows TEM image of nanotubes with the rough surface Volmer-Weber type of grown obtained by using $PtCl_2$ as precursor and BDAC as surfactant.

As Pt surfaces are known to be excellent catalysts, we wanted to test the surface reactivity of different type of engineered Pt NC surfaces. We compared three different type of particles with different type of Pt NCs: i) rough surfaces produced by a Volmer-Weber growth, similar to those reported by Zhang et al.[40], ii) smooth ones (PtAg@Pt nanoboxes) produced by strained epitaxial growth, and iii) treated commercial Pt Black. Note that here rough surfaces display high atomic coordination and low crystallographic index planes while smooth surfaces show low atomic coordination and very high crystallographic index planes. We use as control material the soluble (colloidally stable) fraction of Pt Black (see methods S.I.), otherwise large crystals and aggregation and would further decrease Pt black performance. The overall reduction of p-nitrophenol (p-NP) to p-aminophenol (p-AP) by sodium borohydride ($NaBH_4$) has been chosen as a model reaction, as established in the literature,[43-45] to evaluate the surface reactivity, related to catalytic capability of our different Pt NCs. This reaction has been proved effective to test the efficacy and selectivity of several noble metal catalysts. [28, 46, 47] The reduction cycles were carried out in the same conditions for all samples and then normalized to NCs concentration, total mass and total surface area (Table S1).

The conversion rate efficiency during 10 consecutive cycles of 25 minutes reduction (with no catalyst purification between each cycle) is shown in **Figure 5** (see experimental details). **Figure 5a** plots the UV-VIS spectra showing the decay of the p-NP signal of normalized absorption in the 300 – 500 nm visible range, where it can be clearly seen how the presence of Pt NCs in the solution leads to the rapid vanishment of the p-NP absorption peak, being faster when the smooth surface (high index planes) PtAg@Pt NCs are used. On the contrary, the signal coming from the p-NP is much more stable in presence of treated Pt Black. An intermediate signal decay behavior is observed when Pt NCs with rough surfaces are used. These different behaviors are very clear when plotting the maximum absorption (at 400 nm) versus time (**Fig. 5b**) for each individual cycle. Here the behavior associated to the different

surface reactivity of the NCs is clearly seen, and translates into faster reaction rates as we engineer the NC's surface. This is properly assessed when calculating the apparent kinetic rate constants (k_{app}), normalized to material mass (cost) and surface area (intrinsic activity per unit area), as plotted in **Fig. 5c-e**. The obtained data was analyzed according to the first-order rate law. The negative natural logarithm of the absorbance at 400 nm was plotted against time and the steepest part of the curve was fitted, the slope of which was considered the apparent rate constant k_{app}. It is clearly shown here the superior surface reactivity (up to two orders of magnitude) and high stability of smooth (high index) surfaces vs. the rough (low index) or controls (Pt Black). Regarding k_{app}, it is important to note its stability and repeatability, indicating the stability of the PtAg@Pt NCs during operation, which allows concluding the absence of sample poisoning in the present conditions. The observed progressive decrease in reaction yield with time is attributed to the increased presence of products in the reaction vial as the number of cycles goes by. Importantly, the k_{app} remains constant throughout all the cycles. Note that despite possessing a well defined Pt surface composition, the presence of Ag in the inner layer as remnant of the original Ag template may also have some contribution on the observed catalytic behavior. According to the literature, the presence of Ag in Pt catalyst may improve, mainly, in their structural robustness after catalytic cycling.[38] Other effects related to modifications of the Fermi levels due to alloying and proximity effects should not be discarded and will be subject of future studies.

Pt NC's stability was further studied by analyzing the morphology and performance of the NCs before and after the reduction cycles and thermal stress. For the later, the NCs, prepared at RT, were boiled at 100 ºC for 24 hours, exposed to e-beam showers (Field Emission 300 keV) of 30 minutes, and under intense artificial sun exposure for 7 consecutive days. In any case, no morphological alteration was detected (see TEM images in **Fig. S9**). Additionally, after purification at the end of the 10 reduction cycles or the thermal processes, recovered

NCs just performed as initially. This observed stability could be related to the pinning of the high-index planes by the underneath strained PtAg alloy and the hollow nature of these NCs (since heat is preferably generated in the bulk and dissipated at the surface). Also, it has been observed how the presence of Ag in Pt stabilizes the Pt nanostructure, what has been attributed to the shift of the d-band center of Pt in PtAg alloys.[38] This is important since nanobox collapse and dealloying during use would be otherwise expected.

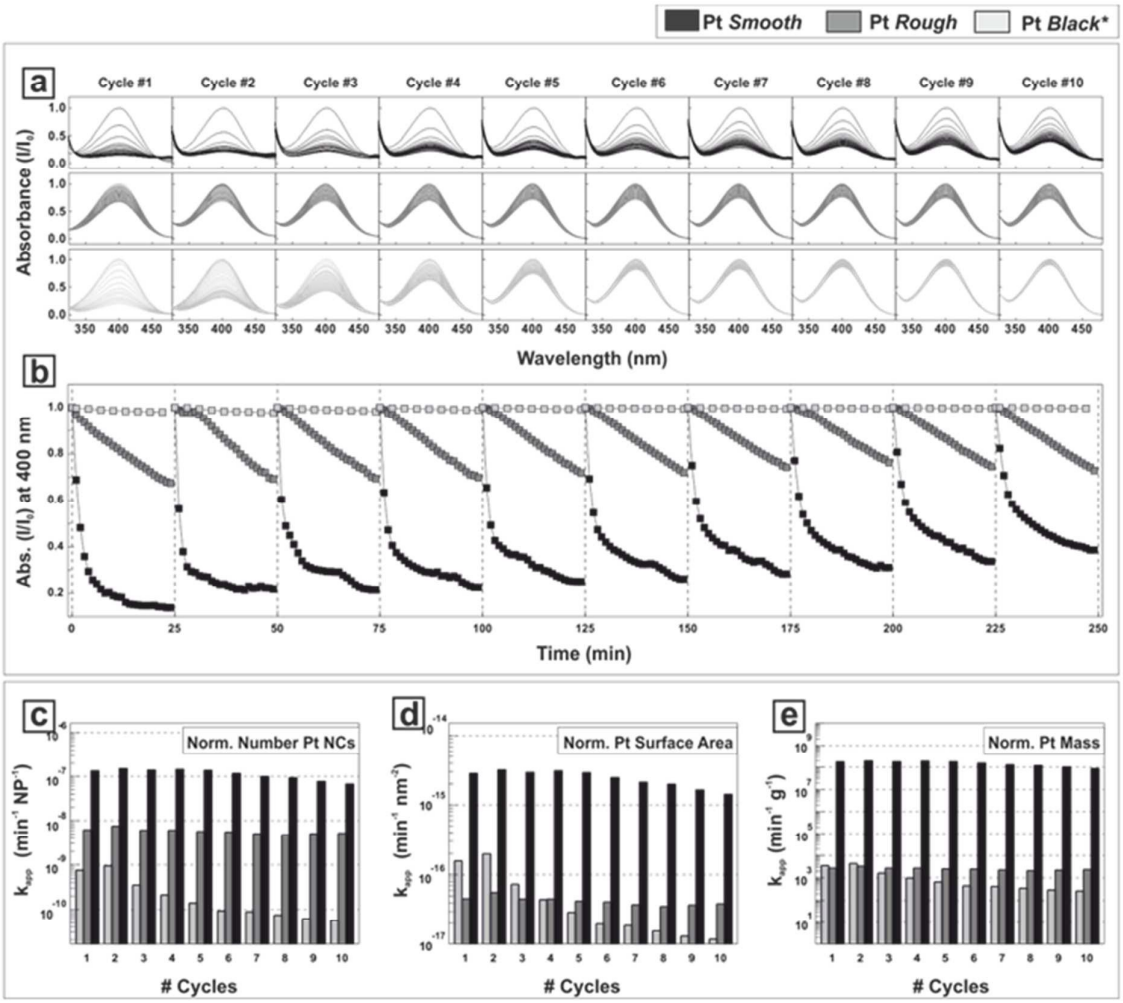

Figure 5. Conversion rate efficiency in the overall degradation of p-nitrophenol into p-aminophenol in the presence of Pt NCs in 10 consecutive 25-minutes reduction cycles.. **a)** Decay of normalized absorbance in the 300-500 nm visible range, indicating the reduction of nitrophenolate ions when using the three different surface shaped PtNCs: Pt 'Smooth', Pt 'Rough' and Pt 'Black*' (*Treated Commercial Pt Black) **b)** Decay of the normalized absorbance at 400 nm. Since the Pt 'Rough' and Pt 'Smooth' catalysed reaction involved the

same amount of total nanoparticles while the Pt 'Black' one had 32 times more (see Table S1), the absorbance of nitrophenolate when using Pt Black was re-normalized (in terms of NCs/mL) for its comparison. The k_{app} values obtained for each PtNC in each reduction cycle were plotted against its respective cycle number after normalizing them as a function of **c)** total number of NCs, **d)** total amount of Pt Surface and **e)** total amount of Pt Mass needed to carry out the reaction.

Summarizing, by slowing down the reaction and controlling Pt dosing, we can obtain a set of Pt NCs with increasing reactivity per unit mass and area. This strategy enables the control of the ratio between Pt and Ag in the alloy with high morphological and structural quality, and the process provides novel insight towards the advanced control of matter at the nanoscale. Finally, this process is also advantageous because it is carried out at room temperature, which results in a more cost-effective and scalable process.

Supporting Information

Details about the preparation, characterization and analysis of the surface of hollow nanocrystals together with the evaluation of the surface reactivity are shown in the Supplementary Information.

Author Information

The authors declare no competing financial interest

Acknowledgements

The authors acknowledge funding from grants 2009 SGR 770, 2009 SGR 776, 2014 SGR 612, 2014 SGR 1638, XaRMAE, CSD2009-00013, MAT2006-13572-C02-02, MAT2009-14734-C02-01, MAT2010-15138, MAT2012-33330, MAT2014-51480-ERC, VALTEC09-2-0085 and VALTEC09-2-0089. J.A. acknowledges NanoAraCat funding for the use of advanced (S)TEM facilities at Instituto de Nanociencia de Aragón–Laboratorio de Microscopia Avanzada. N.G.B. acknowledges financial support through the Juan de la Cierva program (JCI-2011-09678) and European Commission for the Career Integration Grant (322153-MINE) Marie Curie Action. A patent application related to this work was filed 14 March 2011 (European Union application number EP11158024.7).

References

1. Somorjai, G. A.; Contreras, A. M.; Montano, M.; Rioux, R. M., Clusters, surfaces, and catalysis. *Proceedings of the National Academy of Sciences* **2006,** 103, (28), 10577-10583.

2. Yu, T.; Kim, D. Y.; Zhang, H.; Xia, Y., Platinum Concave Nanocubes with High-Index Facets and Their Enhanced Activity for Oxygen Reduction Reaction. *Angewandte Chemie International Edition* **2011,** 50, (12), 2773-2777.

3. Porter, N. S.; Wu, H.; Quan, Z.; Fang, J., Shape-Control and Electrocatalytic Activity-Enhancement of Pt-Based Bimetallic Nanocrystals. *Accounts of Chemical Research* **2013,** 46, (8), 1867-1877.

4. Gu, J.; Zhang, Y.-W.; Tao, F., Shape control of bimetallic nanocatalysts through well-designed colloidal chemistry approaches. *Chemical Society Reviews* **2012,** 41, (24), 8050-8065.

5. Chen, J.; Lim, B.; Lee, E. P.; Xia, Y., Shape-controlled synthesis of platinum nanocrystals for catalytic and electrocatalytic applications. *Nano Today* **2009,** 4, (1), 81-95.

6. Wu, J.; Yang, H., Platinum-Based Oxygen Reduction Electrocatalysts. *Accounts of Chemical Research* **2013,** 46, (8), 1848-1857.

7. Zhang, H.; Jin, M.; Xia, Y., Enhancing the catalytic and electrocatalytic properties of Pt-based catalysts by forming bimetallic nanocrystals with Pd. *Chemical Society Reviews* **2012,** 41, (24), 8035-8049.

8. De Bruijn, F.; Dam, V.; Janssen, G., Review: durability and degradation issues of PEM fuel cell components. *Fuel Cells* **2008,** 8, (1), 3.

9. Xia, X.; Wang, Y.; Ruditskiy, A.; Xia, Y., 25th Anniversary Article: Galvanic Replacement: A Simple and Versatile Route to Hollow Nanostructures with Tunable and Well-Controlled Properties. *Advanced Materials* **2013,** 25, (44), 6313-6333.

10. Chen, Z.; Waje, M.; Li, W.; Yan, Y., Supportless Pt and PtPd Nanotubes as Electrocatalysts for Oxygen-Reduction Reactions. *Angewandte Chemie International Edition* **2007,** 46, (22), 4060-4063.

11. Chen, H. M.; Liu, R.-S.; Lo, M.-Y.; Chang, S.-C.; Tsai, L.-D.; Peng, Y.-M.; Lee, J.-F., Hollow Platinum Spheres with Nano-Channels: Synthesis and Enhanced Catalysis for Oxygen Reduction. *The Journal of Physical Chemistry C* **2008,** 112, (20), 7522-7526.

12. Liang, H.-P.; Zhang, H.-M.; Hu, J.-S.; Guo, Y.-G.; Wan, L.-J.; Bai, C.-L., Pt Hollow Nanospheres: Facile Synthesis and Enhanced Electrocatalysts. *Angewandte Chemie* **2004,** 116, (12), 1566-1569.

13. Chen, J.; Wiley, B.; McLellan, J.; Xiong, Y.; Li, Z.-Y.; Xia, Y., Optical Properties of Pd−Ag and Pt−Ag Nanoboxes Synthesized via Galvanic Replacement Reactions. *Nano Letters* **2005,** 5, (10), 2058-2062.

14. Lim, B.; Jiang, M.; Camargo, P. H. C.; Cho, E. C.; Tao, J.; Lu, X.; Zhu, Y.; Xia, Y., Pd-Pt Bimetallic Nanodendrites with High Activity for Oxygen Reduction. *Science* **2009,** 324, (5932), 1302-1305.

15. Wang, L.; Yamauchi, Y., Metallic Nanocages: Synthesis of Bimetallic Pt–Pd Hollow Nanoparticles with Dendritic Shells by Selective Chemical Etching. *Journal of the American Chemical Society* **2013,** 135, (45), 16762-16765.

16. Zhang, L.; Roling, L. T.; Wang, X.; Vara, M.; Chi, M.; Liu, J.; Choi, S.-I.; Park, J.; Herron, J. A.; Xie, Z.; Mavrikakis, M.; Xia, Y., Platinum-based nanocages with subnanometer-thick walls and well-defined, controllable facets. *Science* **2015,** 349, (6246), 412-416.

17. Tian, N.; Zhou, Z.-Y.; Sun, S.-G.; Ding, Y.; Wang, Z. L., Synthesis of Tetrahexahedral Platinum Nanocrystals with High-Index Facets and High Electro-Oxidation Activity. *Science* **2007,** 316, (5825), 732-735.

18. Xia, B. Y.; Wu, H. B.; Wang, X.; Lou, X. W., Highly Concave Platinum Nanoframes with High-Index Facets and Enhanced Electrocatalytic Properties. *Angewandte Chemie International Edition* **2013,** 52, (47), 12337-12340.

19. González, E.; Arbiol, J.; Puntes, V. F., Carving at the Nanoscale: Sequential Galvanic Exchange and Kirkendall Growth at Room Temperature. *Science* **2011,** 334, (6061), 1377-1380.

20. Yin, Y.; Rioux, R. M.; Erdonmez, C. K.; Hughes, S.; Somorjai, G. A.; Alivisatos, A. P., Formation of Hollow Nanocrystals Through the Nanoscale Kirkendall Effect. *Science* **2004,** 304, (5671), 711-714.

21. Yin, Y.; Erdonmez, C. K.; Cabot, A.; Hughes, S.; Alivisatos, A. P., Colloidal Synthesis of Hollow Cobalt Sulfide Nanocrystals. *Advanced Functional Materials* **2006,** 16, (11), 1389-1399.

22. Wiley, B.; Herricks, T.; Sun, Y.; Xia, Y., Polyol Synthesis of Silver Nanoparticles: Use of Chloride and Oxygen to Promote the Formation of Single-Crystal, Truncated Cubes and Tetrahedrons. *Nano Letters* **2004,** 4, (9), 1733-1739.

23. Catalan, G.; Lubk, A.; Vlooswijk, A. H. G.; Snoeck, E.; Magen, C.; Janssens, A.; Rispens, G.; Rijnders, G.; Blank, D. H. A.; Noheda, B., Flexoelectric rotation of polarization in ferroelectric thin films. *Nat Mater* **2011,** 10, (12), 963-967.

24. Guisbiers, G., Schottky Defects in Nanoparticles. *The Journal of Physical Chemistry C* **2011,** 115, (6), 2616-2621.

25. Yin, Y.; Alivisatos, A. P., Colloidal nanocrystal synthesis and the organic-inorganic interface. *Nature* **2005,** 437, (7059), 664-670.

26. Penn, R. L.; Banfield, J. F., Imperfect Oriented Attachment: Dislocation Generation in Defect-Free Nanocrystals. *Science* **1998,** 281, (5379), 969-971.

27. Yu, Y.; Zhang, Q.; Yao, Q.; Xie, J.; Lee, J. Y., Architectural Design of Heterogeneous Metallic Nanocrystals—Principles and Processes. *Accounts of Chemical Research* **2014,** 47, (12), 3530-3540.

28. Bastús, N. G.; Merkoçi, F.; Piella, J.; Puntes, V., Synthesis of Highly Monodisperse Citrate-Stabilized Silver Nanoparticles of up to 200 nm: Kinetic Control and Catalytic Properties. *Chemistry of Materials* **2014,** 26, (9), 2836-2846.

29. Lou, X. W.; Archer, L. A.; Yang, Z., Hollow Micro-/Nanostructures: Synthesis and Applications. *Advanced Materials* **2008,** 20, (21), 3987-4019.

30. Chen, J.; Wiley, B.; Li, Z. Y.; Campbell, D.; Saeki, F.; Cang, H.; Au, L.; Lee, J.; Li, X.; Xia, Y., Gold Nanocages: Engineering Their Structure for Biomedical Applications. *Advanced Materials* **2005,** 17, (18), 2255-2261.

31. Gao, J.; Ren, X.; Chen, D.; Tang, F.; Ren, J., Bimetallic Ag–Pt hollow nanoparticles: Synthesis and tunable surface plasmon resonance. *Scripta Materialia* **2007,** 57, (8), 687-690.

32. Zhang, Q.; Xie, J.; Lee, J. Y.; Zhang, J.; Boothroyd, C., Synthesis of Ag@AgAu Metal Core/Alloy Shell Bimetallic Nanoparticles with Tunable Shell Compositions by a Galvanic Replacement Reaction. *Small* **2008,** 4, (8), 1067-1071.

33. Liz-Marzan, L. M.; Philipse, A. P., Stable hydrosols of metallic and bimetallic nanoparticles immobilized on imogolite fibers. *The Journal of Physical Chemistry* **1995,** 99, (41), 15120-15128.

34. Somorjai, G. A.; Blakely, D. W., Mechanism of catalysis of hydrocarbon reactions by platinum surfaces. *Nature* **1975,** 258, (5536), 580-583.

35. Chang, L. Y.; Barnard, A. S.; Gontard, L. C.; Dunin-Borkowski, R. E., Resolving the Structure of Active Sites on Platinum Catalytic Nanoparticles. *Nano Letters* **2010,** 10, (8), 3073-3076.

36. Lim, S. I.; Ojea-Jimenez, I.; Varon, M.; Casals, E.; Arbiol, J.; Puntes, V., Synthesis of Platinum Cubes, Polypods, Cuboctahedrons, and Raspberries Assisted by Cobalt Nanocrystals. *Nano Letters* **2010,** 10, (3), 964-973.

37. Wanjala, B. N.; Luo, J.; Loukrakpam, R.; Fang, B.; Mott, D.; Njoki, P. N.; Engelhard, M.; Naslund, H. R.; Wu, J. K.; Wang, L.; Malis, O.; Zhong, C.-J., Nanoscale Alloying, Phase-Segregation, and Core−Shell Evolution of Gold−Platinum Nanoparticles and Their Electrocatalytic Effect on Oxygen Reduction Reaction. *Chemistry of Materials* **2010,** 22, (14), 4282-4294.

38. Peng, Z.; You, H.; Yang, H., An Electrochemical Approach to PtAg Alloy Nanostructures Rich in Pt at the Surface. *Advanced Functional Materials* **2010,** 20, (21), 3734-3741.

39. Peng, Z.; Yang, H., Ag–Pt alloy nanoparticles with the compositions in the miscibility gap. *Journal of Solid State Chemistry* **2008,** 181, (7), 1546-1551.

40. Zhang, W.; Yang, J.; Lu, X., Tailoring Galvanic Replacement Reaction for the Preparation of Pt/Ag Bimetallic Hollow Nanostructures with Controlled Number of Voids. *ACS Nano* **2012,** 6, (8), 7397-7405.

41. Sun, Y.; Xia, Y., Shape-Controlled Synthesis of Gold and Silver Nanoparticles. *Science* **2002,** 298, (5601), 2176-2179.

42. Ferreira, P. J.; la O', G. J.; Shao-Horn, Y.; Morgan, D.; Makharia, R.; Kocha, S.; Gasteiger, H. A., Instability of Pt/C Electrocatalysts in Proton Exchange Membrane Fuel Cells: A Mechanistic Investigation. *Journal of the Electrochemical Society* **2005,** 152, (11), A2256-A2271.

43. Shen, Y.-Y.; Sun, Y.; Zhou, L.-N.; Li, Y.-J.; Yeung, E. S., Synthesis of ultrathin PtPdBi nanowire and its enhanced catalytic activity towards p-nitrophenol reduction. *Journal of Materials Chemistry A* **2014,** 2, (9), 2977-2984.

44. Zeng, J.; Zhang, Q.; Chen, J.; Xia, Y., A Comparison Study of the Catalytic Properties of Au-Based Nanocages, Nanoboxes, and Nanoparticles. *Nano Letters* **2009,** 10, (1), 30-35.

45. Qin, G. W.; Pei, W.; Ma, X.; Xu, X.; Ren, Y.; Sun, W.; Zuo, L., Enhanced Catalytic Activity of Pt Nanomaterials: From Monodisperse Nanoparticles to Self-Organized Nanoparticle-Linked Nanowires. *The Journal of Physical Chemistry C* **2010,** 114, (15), 6909-6913.

46. Yu, T.; Zeng, J.; Lim, B.; Xia, Y., Aqueous-Phase Synthesis of Pt/CeO2 Hybrid Nanostructures and Their Catalytic Properties. *Advanced Materials* **2010,** 22, (45), 5188-5192.

47. Yu, X.; Shavel, A.; An, X.; Luo, Z.; Ibañez, M.; Cabot, A., Cu2ZnSnS4-Pt and Cu2ZnSnS4-Au Heterostructured Nanoparticles for Photocatalytic Water Splitting and Pollutant Degradation. *Journal of the American Chemical Society* **2014,** 136, (26), 9236-9239.

Graphical Abstract

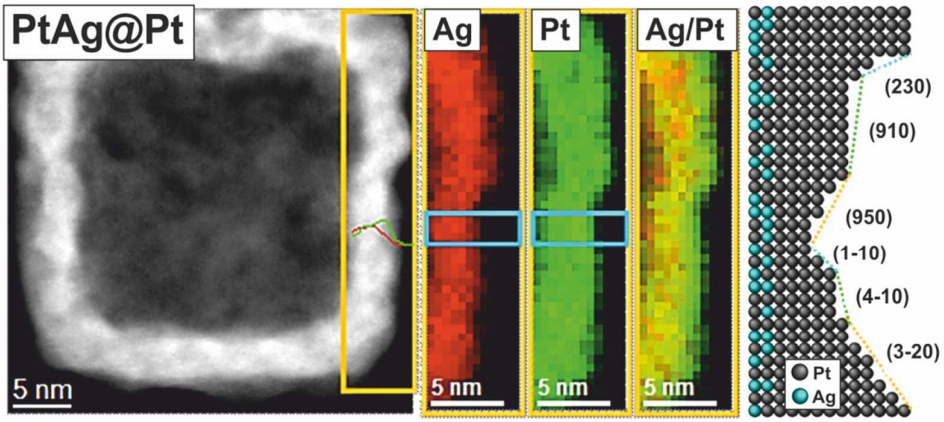

A novel synthetic strategy based on the controlled corrosion of silver templates allow to prepare PtAg@Pt single-crystal hollow NCs with high-index planes at room temperature with enhanced surface reactivity.